Thermal Maps of Jupiter: Spatial Organization and Time Dependence of Stratospheric Temperatures, 1980 to 1990

GLENN S. ORTON, A. JAMES FRIEDSON, JOHN CALDWELL, HEIDI B. HAMMEL, KEVIN H. BAINES, JAY T. BERGSTRALH, TERRY Z. MARTIN, MICHAEL E. MALCOM, ROBERT A. WEST, WILLIAM F. GOLISCH, DAVID M. GRIEP, CHARLES D. KAMINSKI, ALAN T. TOKUNAGA, RICHARD BARON, MARK SHURE

The spatial organization and time dependence of Jupiter's stratospheric temperatures have been measured by observing thermal emission from the 7.8-micrometer CH_4 band. These temperatures, observed through the greater part of a Jovian year, exhibit the influence of seasonal radiative forcing. Distinct bands of high temperature are located at the poles and mid-latitudes, while the equator alternates between warm and cold with a period of approximately 4 years. Substantial longitudinal variability is often observed within the warm mid-latitude bands, and occasionally elsewhere on the planet. This variability includes small, localized structures, as well as large-scale waves with wavelengths longer than ~30,000 kilometers. The amplitudes of the waves vary on a time scale of ~1 month; structures on a smaller scale may have lifetimes of only days. Waves observed in 1985, 1987, and 1988 propagated with group velocities less than ±30 meters per second.

THE BRIGHTNESS AND COLORS OF JUPITER'S CLOUD SYSTEM have been studied at visible wavelengths for centuries, yielding information about cloud properties and winds in the troposphere. In contrast, the stratosphere has received comparatively little attention. Measurements of the thermal structure of this region are important for a number of reasons. For example, the difference between tropospheric and stratospheric horizontal variations of thermal structure provides clues about the mechanisms governing dominant spatial scales and temporal variability. In addition, observations of stratospheric waves may supply new information about the physical properties of waves in the troposphere. As tropospheric waves propagate upward, their amplitude increases with height. Thus, small amplitude waves which may be difficult or impossible to detect thermally in the troposphere become easier to detect in the stratosphere. Finally, the thermal structure of the stratosphere is coupled to its global circulation, and knowledge of this circulation is essential for estimating the effect of mass motions on the spatial distribution of aerosols and trace species.

Measurement of the stratospheric structure and composition requires observations of thermal infrared emission or analysis of infrequent stellar occultations. Ground-based infrared observations are generally more difficult to obtain than those made at visible wavelengths. As a consequence, previous reconnaissance of the stratosphere has been mostly confined to brief examinations by interplanetary spacecraft or stellar occultations (*1–3*), which have yielded only limited information concerning the spatial organization and time dependence of Jupiter's stratospheric temperatures. This article describes initial results derived from ground-based observations of thermal emission at 7.8 μm. The observations comprise the most extensive investigation of the stratosphere carried out to date, combining broad spatial coverage with a 10-year baseline of measurements. They reveal that stratospheric temperatures exhibit considerable spatial and temporal variability (Fig. 1).

We observed Jupiter between 1980 and 1990 at the NASA Infrared Telescope Facility on Mauna Kea, Hawaii. Stratospheric temperatures are determined from thermal infrared emission observed through a filter centered on the strong CH_4 ν_4 vibration-rotation band between 1250 and 1350 cm^{-1}. Because methane is uniformly mixed to high altitude (*4*), observed variations of CH_4 emission arise from variations of temperature rather than from CH_4 abundance.

Only scans along Jupiter's central meridian were made prior to 1984. Afterward, images were constructed by raster-scanning, sampling the disk in a rectangular grid at 1-arc sec intervals. The diameter of the circular aperture used in 1980 and 1981 was 3.92 arc sec. For later observations, it was 1.96 arc sec, corresponding to 5° of latitude or longitude or 6600 km at the equator at opposition. The procedure to assign planetocentric latitude, longitude, and emission angle to each pixel of an image accounts for drift of the telescope from the actual motion of Jupiter in the sky and for planetary rotation during the approximately 45 minutes required to complete a raster scan.

G. S. Orton, A. J. Friedson, K. H. Baines, T. Z. Martin, and R. A. West are at the Jet Propulsion Laboratory, California Institute of Technology, 4800 Oak Grove Drive, Pasadena, CA 91109. J. Caldwell is in the Physics Department, York University, 4700 Keele Street, North York, Ontario, M3J 1P3, Canada. H. B. Hammell is in the Department of Earth, Atmospheric and Planetary Sciences, Massachusetts Institute of Technology, Cambridge, MA 02139. J. T. Bergstralh is at the National Aeronautics and Space Administration, Washington, DC 20546. M. E. Malcom is at TRW, 1 Space Park, Redondo Beach, CA 90278. W. F. Golisch, D. M. Griep, C. D. Kaminski, A. T. Tokunaga, R. Baron, and M. Shure are at the Institute for Astronomy, University of Hawaii, 2680 Woodlawn Drive, Honolulu, HI 96822.

Motion between Earth and an observation point on Jupiter causes a Doppler shift of Jovian CH_4 emission lines relative to CH_4 absorption lines in the terrestrial atmosphere. As a result, the value of thermal emission measured with our filter depends on the line-of-sight relative velocity between the telescope and the emitting gas. This effect alters the intensity by as much as 38 percent over the range of relative velocities encountered in the measurements. The intensity of each pixel of an image was corrected for the dependence of telluric CH_4 extinction on radial velocity (although the raw images presented in Figs. 1 and 6 do not incorporate this correction).

Intensities were calibrated by equating the mean value observed in the inner 50 percent of a strip centered on Jupiter's central meridian to that observed by the Voyager 1 infrared spectrometer (IRIS) central meridian ("north-south") maps in a simulated response to our filter. As a result, our data are insensitive to temporal variations of the global mean temperature, but retain sensitivity to relative variations of temperature in latitude and longitude. The best images have a signal-to-noise ratio of 40 to 55 (equivalent to a brightness temperature uncertainty of 0.2 to 0.3 K), depending on whether the signal represents a warm or cool feature. Noisier images result from increased humidity and attenuation of signal by telluric water vapor or from extremely poor seeing.

The contribution function for the 7.8-μm measurements is shown in Fig. 2. This function measures the relative contribution made by each atmospheric level to the total outgoing thermal radiance. Its width in altitude indicates the relatively poor vertical resolution inherent in these measurements of stratospheric temperature. In order to interpret intensities in terms of physical temperature under these circumstances, some assumption must be made concerning the average vertical thermal structure of the atmosphere. Once a baseline vertical structure has been established, horizontal variations in the source of thermal emission are considered to arise from small deviations of the local temperature from the baseline value.

The Voyager 1 and 2 Radio Science Subsystem (RSS) experiments (*2*) provided temperature profiles between 1 bar and 1 mbar pressure, near the equator and near 70°S latitude, which we used as a guide for estimating the global average vertical structure. However, the large location- and time-dependence among these results, such as the 30 K range of temperatures at the 30-mbar level, suggested that adopting a single "universal" vertical structure would not be meaningful. We imposed a further requirement that the baseline profile provide a good fit to the emission angle and radial velocity dependence of 7.8-μm measurements taken in a strip along the equator. The equator was chosen because it generally exhibits very little zonal (east-west) structure, thereby assuring as much as possible that intensity variations arise strictly from emission angle and radial velocity effects. The baseline temperature profile shown in Fig. 2 provided an acceptable fit to the equatorial center-to-limb brightness variation for most of the data acquired between 1985 and 1990. However, the center-to-limb variation of 1984 and 1987 measurements were not fit well by this temperature structure. The alternative baseline profile shown in Fig. 2 was found to provide a better fit for these data. The first profile is qualitatively similar to the Voyager 1 RSS ingress occultation profile in that it is relatively warm at 30 mbar and has a low average lapse rate between 50 and 1 mbar, while the second profile is similar to the Voyager 1 egress profile. We cannot separate the emission angle and radial velocity dependence of intensity from true source variations for the central meridian scans of 1980 to 1983. For these data, we simply assumed that the baseline profile was adequately given by the temperature structure shown as the thin solid line in Fig. 2.

To interpret 7.8-μm intensities in terms of physical temperature, we constructed a family of temperature profiles which correspond to a series of continuous perturbations to a baseline profile. The perturbation profiles were parameterized in the following form:

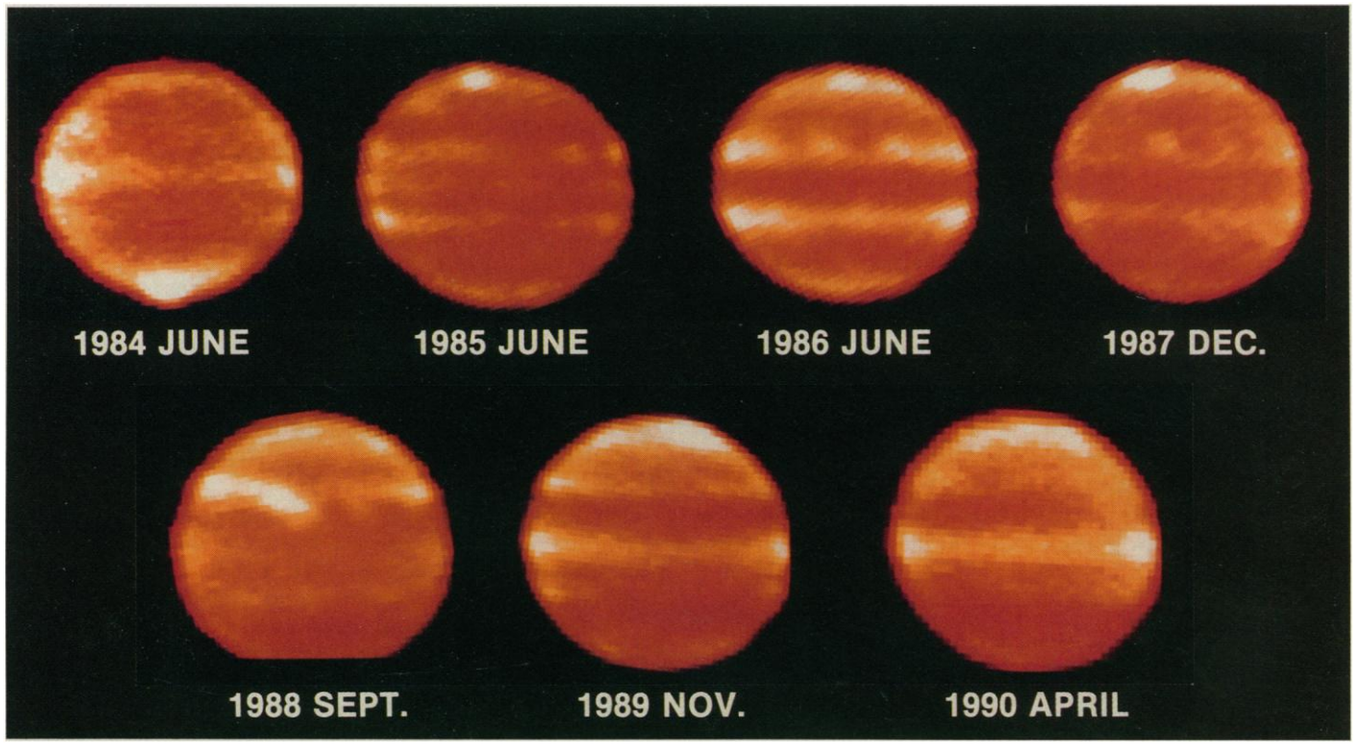

Fig. 1. Representative raster-scan images of Jupiter at 7.8 μm, observed at seven different times between June 1984 and April 1990, identified by the epoch of observation. The color key has been stretched to show detail at the expense of saturating the image at the bright north and south polar hot spots.

$$T_p(z) = T_0(z) + \frac{T(1\text{ mbar}) - T_0(1\text{ mbar})}{z(1\text{ mbar}) - z(100\text{ mbar})}[z - z(100\text{ mbar})] \quad (1)$$

Here, T_p is the perturbation temperature, T_0 is the baseline temperature, z is altitude, and $T(1\text{ mbar})$ is the free parameter that characterizes the magnitude of the deviation from the baseline profile. Each perturbation profile has the same 100-mbar temperature as the baseline profile but a different 1-mbar temperature, and the difference between the two profiles varies linearly with height. Line-by-line calculations were performed to construct a one-to-one mapping between the free parameter $T(1\text{ mbar})$ and the corresponding outgoing 7.8-μm intensity produced for a range of emission angles and radial velocities. This mapping was used to link a perturbation temperature profile to the intensity at each pixel of a scan or map. Temperatures derived with this scheme are reported in terms of the value at the 20-mbar level when the standard baseline profile was used, and in terms of the value at the 10-mbar level when the alternate baseline profile was used (for the years 1984 and 1987). The 20-mbar and 10-mbar pressure levels represent altitudes close to the peak of the contribution functions for the standard and alternate baseline profiles, respectively.

Two types of systematic error influence our results. The first arises from the absolute calibration, and we have no quantitative estimate of the magnitude of the error introduced by scaling 7.8-μm intensities to the 1979 Voyager IRIS results. The second arises from uncertainty of the vertical temperature profile in Jupiter's stratosphere as a function of position and time. Absorption by telluric CH_4 obscures the variation of intensity with emission angle by introducing an additional dependence of intensity on the radial velocity between the emitting source and the observer. A full correction for emission angle and radial velocity effects requires precise knowledge of the vertical temperature structure at all locations and times, which we clearly do not have. Instead, we compute our correction using the baseline temperature profiles shown in Fig. 2. A useful estimate of the error introduced by this approximation is obtained by examining differences in temperatures derived for the same location from different maps. These differences range from less than 0.5 K to about 4 K in maps where overlapping coverage is available. The uncertainty between temperatures derived from locations close to one another in the same image, having nearly the same emission angle and radial velocity, arises simply from observational noise and is as small as 0.2 to 0.3 K.

Zonal mean thermal structure. The zonal mean 20-mbar temperature as a function of latitude is shown for the years 1980 to 1990 in Fig. 3. Most of these profiles were constructed from separate images which together covered the full range of longitude and which all were acquired within a period of three days or less. However, for 1981 to 1984, 1986, and 1990, the longitudinal coverage contained large gaps. The 1983 data, in fact, represent the average of only two central-meridian scans.

The radiatively forced seasonal asymmetry between northern and southern hemispheres is apparent in Fig. 3, despite the small (3°) axial tilt. The time dependence of temperature shows a northern temperature maximum and southern minimum near northern summer solstice (1988.7), some 2 years earlier than expected from modeling the purely radiative response to seasonal forcing (7). If future data confirm this trend, then additional control of stratospheric temperatures, perhaps by photochemistry or dynamics, is implied. The absence of a clear southern maximum and northern minimum may be the result of hemispherically asymmetric insolation arising from Jupiter's orbital eccentricity (*8*).

Superimposed on the seasonal hemispheric asymmetry is a series of warm and cold bands. Between 1980 and 1987, local maxima in the zonal mean temperature existed consistently near 20°S and 20°N planetocentric latitude, while the equator alternated between being warm and cold (Fig. 3). This pattern was also present in 1977 scans of Jupiter by Sinton *et al.* (*5*), in 1979 Voyager 1 IRIS north-south map data of CH_4 band emission, and in ground-based data contemporary with the Voyager encounters by Caldwell *et al.* (*6*). The mid-latitude warm bands are located near the positions of annual average stratospheric temperature maxima predicted by Conrath *et al.* (*9*). During 1988, the northern mid-latitude temperature maximum moved from 20° to 30°N.

The temporal variation of the position and relative amplitude of the bands can be described as a continuous cycle between two

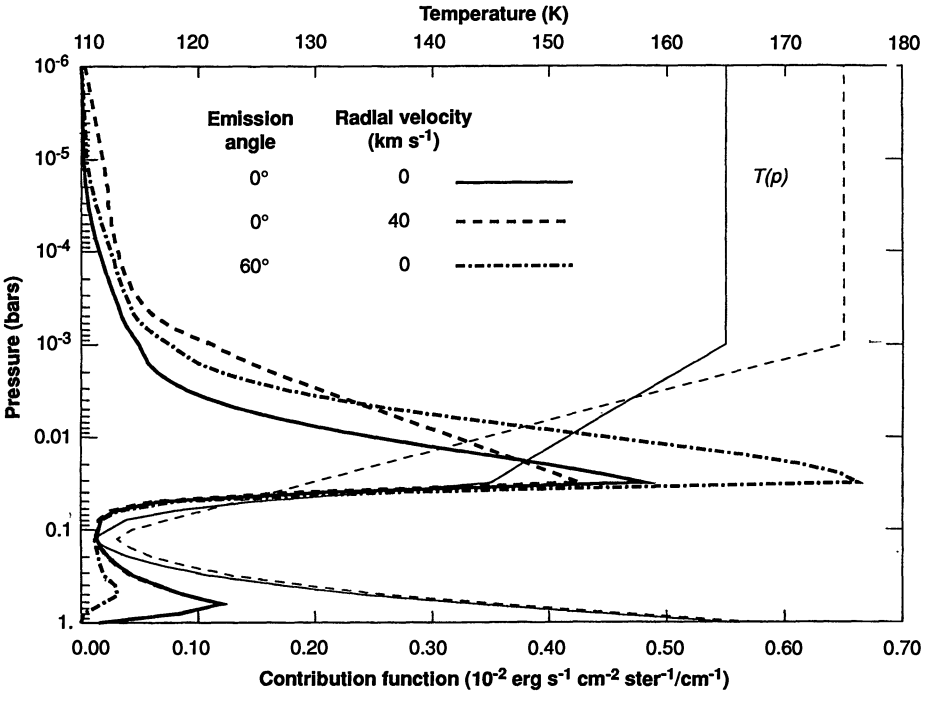

Fig. 2. Plot of the level-by-level contribution to the outgoing thermal intensity as a function of height for the baseline temperature profile given by the thin solid line. An alternative temperature profile given as the thin dashed line was used for data taken in 1984 and in 1987. Contribution functions are shown for three different cases of observed emission angle and radial velocity. The abscissa plots the outgoing intensity per (unitless) decimal logarithm of pressure (in bars). The discontinuities of the temperature structure slope are artificial and simply reflect the crudeness of our current understanding of the vertical structure.

end-member states, one with the equator as the warmest latitude (such as in 1980, 1984, and 1989), the other with only two warm bands at ±20° latitude situated about a cold equator (such as in 1982 and 1986). Temperatures appear to cycle between these states with a period of roughly 4 years, but a longer baseline of data is needed to verify the periodic nature of the equatorial temperature.

In Jupiter's troposphere, temperatures correlate strongly with visible albedo variations. However, there is no evident link of stratospheric temperatures to the visible albedo pattern, either for the zonal mean structure or for individual features. This rules out the possibility that meridional stratospheric temperature variations are created by heating caused by horizontally inhomogeneous reflected sunlight or thermal emission from the troposphere (*10*). Therefore, it is apparent that dynamics assumes an important role in the stratosphere, either directly through local heat transport, or indirectly by inducing aerosol or chemical constituent variations that cause local solar heating to vary. It has been proposed that the upper tropospheric and stratospheric thermal structure of Jupiter is driven away from radiative equilibrium by dynamical forcing associated with a time-variable circulation pattern (*9*). If this is the case, then periods characterized by a cold equator and warm mid-latitudes correspond to a circulation pattern having zonal mean upwelling and adiabatic cooling occurring at the equator, and subsidence and adiabatic warming at middle latitudes. A circulation flowing in the opposite sense would pertain during times when the equator is warm.

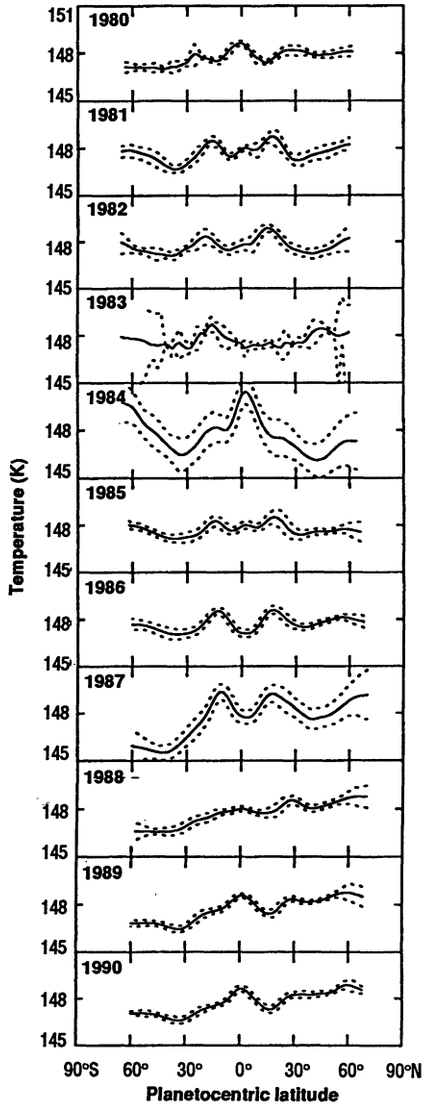

Fig. 3. Derived zonal mean temperatures at 20-mbar total pressure (for all years except 1984 and 1987) and at 10-mbar pressure (for 1984 and 1987), as a function of latitude. Zonal mean temperatures are plotted as solid curves; the dotted curves above and below represent one standard deviation characterizing the variance of temperatures about the mean at each latitude. This variance is composed both of true longitudinal fluctuations and of noise fluctuations. Note the seasonal hemispherical asymmetry, the presence of mid-latitude warm bands, and the oscillation of the equatorial temperature.

Longitudinal structure. Substantial longitudinal structure appears in nearly all of the maps from 1984 to the present (Fig. 1). Voyager 1 IRIS maps at 7.8 μm were too noisy for the purposes of studying zonal structure. There are indications of longitudinal variations when separate central meridian scans are pieced together (Fig. 4), although the uncertainty in positioning the individual scans on Jupiter's disk precludes a more quantitative analysis. Several of the images in Fig. 1 and the 1981 map in Fig. 4 clearly reveal the north polar hot spot near 180°W longitude, a feature associated with the magnetic field and possibly related to auroral phenomena. This feature and its southern counterpart (also visible in Fig. 1 and at various longitudes in Fig. 4) have been discussed already elsewhere (*11*).

Between 1984 and 1988, most images showed longitudinal temperature oscillations, predominantly at the latitudes of the warm bands (Fig. 1). In contrast, no wave-like activity was observed in 1989 and 1990. In general, wave activity is more pronounced in the northern than in the southern hemisphere, and the waves are, for the most part, confined to a band extending from ~15°N to 30°N latitude.

Planetary-scale waves are particularly evident at subtropical latitudes in data taken in June 1985 and in September and November 1988. Similar waves with reduced amplitude were observed during June and July 1986 and October and December 1987. One outstanding example, centered at 22°N planetocentric latitude, was observed in September 1988 and again in November and December (Fig. 5). The hottest feature in the wave extends over ~15,000 km and reaches ~2 K above the ambient 20-mbar zonal mean temperature. It is followed by a wave train, confined between 15° and 30°N. A discrete Fourier transform analysis shows that the predominant zonal Fourier component corresponds to wavenumber 11. A qualitatively similar structure was still observed in November, but the Fourier components of the wave varied considerably in amplitude and phase during the intervening time. The time over which these components doubled or halved their amplitude was ~50 Jovian rotations (~20 terrestrial days).

It is difficult to determine the dispersion relation that relates the phase speed (measured relative to the local zonal wind) to wavenumber for the wave observed in 1988, as we have no information regarding its vertical structure or the zonal mean wind in which it is embedded. In addition, the total energy associated with the wave changed substantially between September and November. During

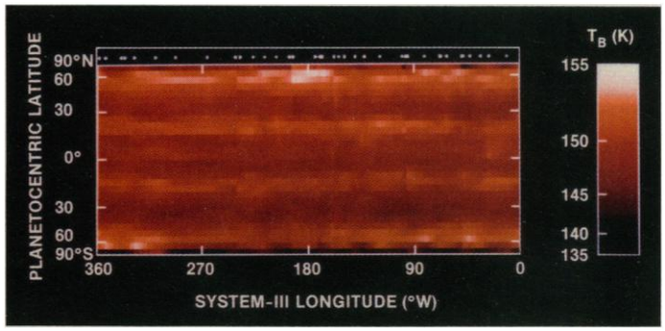

Fig. 4. A 7.8-μm cylindrical map, obtained from linear interpolation of 38 central meridian scans taken on 19 to 23 March 1981. White dots above the map indicate the System III longitude position of each central meridian scan. The intensity scale is linear and is shown in a key which is referenced to equivalent brightness temperatures.

this period, changes in the wave structure were caused both by its dispersive horizontal propagation and by nonconservative forcing, damping, or instability. Unambiguous measurement of the horizontal group velocity requires the ability to distinguish between these effects. Consequently, observations taken no more than a few days apart should be used, in order to minimize the contributions of nonconservative processes. We found no measurable longitudinal displacements of features in data taken 2 days apart in June 1985, December 1987, and September and November 1988. This finding sets an upper limit of ± 30 m s^{-1} on the zonal group velocity of these waves relative to System III, the coordinate system rotating at the same rate as Jupiter's magnetic field. This upper limit does not strongly constrain the dispersion relation without further information regarding the local zonal mean wind.

The fact that stratospheric planetary waves have their largest amplitudes at $\pm 20°$ latitude may be significant, as this is where large-scale zonal variations of temperature in the upper troposphere were prominent in Voyager data (*12*). It has been suggested that these tropospheric thermal fluctuations are related to the retrograde jets at $\pm 18°$ planetocentric latitude in Jupiter's troposphere, which are expected to be highly susceptible to instability associated with their horizontal wind shear (*13*). It is possible that the stratospheric waves originate as instabilities in the troposphere and propagate vertically upward, increasing their amplitude along the way as the background atmospheric density decreases with altitude. If this is correct, then continued observation and modeling of these waves may prove to be a powerful tool for probing the nature of jet instability and wave excitation mechanisms in the troposphere.

Other zonally asymmetric features present in the images are small warm regions that appear to be spatially localized rather than harmonic in nature. Striking small-scale features were observed on 6 August 1984 at the equator and on 21 June 1985 between 14° and 30°S (Fig. 6). These narrow, curved structures were seen in enhanced thermal emission near the Jovian limb. The 1984 feature was at least 38,000 km in length; the 1985 feature was segmented, with two parts of length 27,000 km (near 15°S) and 24,000 km (Fig. 6). As a consequence of irregular temporal sampling of the planet, it is possible only to characterize their lifetime as having been greater than 2 hours and less than 4 to 5 weeks. The maximum amplitudes of both features were about 1.0 to 1.5 K above the surrounding ambient temperature. Similar features can be seen in images up through 1988 (see the images in Fig. 1 for December 1987 and September 1988) but none since.

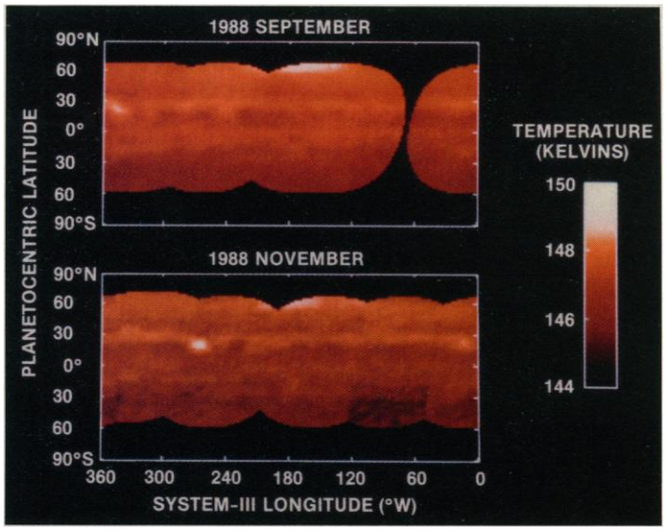

Fig. 5. Cylindrical map of 20-mbar stratospheric temperatures for 25, 26, and 28 September 1988 (top) and 30 November to 2 December (bottom). Temperatures were derived from six separate images in September and five in November. Intensities of pixels in the original images were interpolated onto the cylindrical map grid with the use of parametric cubic convolution (*15*). Temperatures were not derived from data with an emission angle greater than 66°. In regions where different images provided overlapping coverage, observations with the lowest emission angle were used. Small discontinuities in the temperature field, particularly evident in the lower map, arise at the boundaries between images. Such discontinuities indicate that the baseline temperature profile used to derive temperatures (see Fig. 2, thin solid line) accounts only approximately for the emission angle and radial velocity dependence of the intensity. Note the striking planetary wave located at 20°N in both maps. One of the images used to derive temperatures in the September map is shown in Fig. 1.

Remaining questions. Our observations of the Jovian stratosphere reveal a meteorology as dynamically active as that of Earth's stratosphere (*14*). Radiative and dynamical processes combine to produce a thermal structure that is highly variable, both spatially and temporally. Some qualitative aspects of the observed temperature field were anticipated in the literature, such as the perennially warm mid-latitude bands (*9*). Other phenomena represent new areas for investigation, including (i) an extremely rapid response to the insolation cycle, (ii) a roughly 4-year periodic oscillation of the equatorial zonal mean temperature, (iii) planetary-scale waves located in the warm mid-latitude bands, and (iv) the infrequent appearance of localized, small-scale warm features. A number of questions related to these phenomena can be posed: What is responsible for driving the oscillation of the equatorial zonal mean temperature? What is the dispersion relation of the planetary-scale waves, what is their source of origin, and how are they related to the frictional drag that causes zonal winds to decay with altitude in the stratosphere (*12*)? What is the origin of the localized, small-scale features?

It is important to reduce the assumptions of this study, elucidating further details of the structure and variability of the vertical temperature profile by examining the effects of emission angle and Doppler shift on the contribution function. Equally important in the immediate future is studying the implications of the measured zonal mean thermal structure for the zonally symmetric component of the stratospheric circulation, for which no other constraints exist. The 7.8-μm data presented here represent only part of a larger program measuring thermal emission from Jupiter and Saturn in several spectral regions. Further analyses of data should provide information concerning temperatures, chemical distributions, and cloud properties in the tropospheres of these planets. Future investigation of the Jovian stratosphere and troposphere should greatly benefit from the use of 5- to 22-μm infrared astronomical cameras, which are under development and testing. We expect these

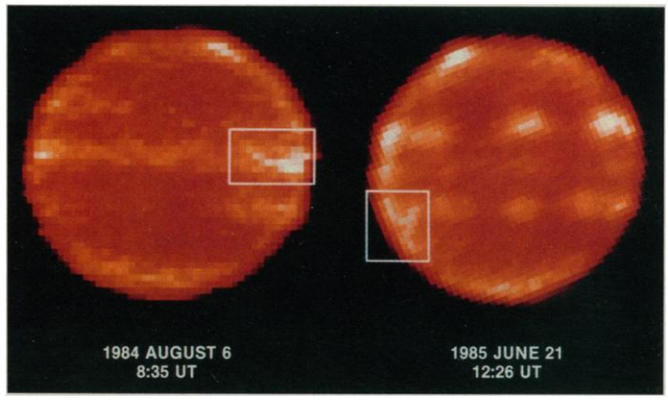

Fig. 6. Raster-scan images of Jupiter at 7.8 μm. Distinct warm features, described in the text, are visible in these images and located within each box. The times given refer to the beginning of each 45-minute observation.

observations to support the data to be acquired by the Galileo mission at Jupiter by providing extended vertical and temporal coverage of atmospheric conditions across the planet.

REFERENCES AND NOTES

1. A. J. Kliore and P. J. Woiceshyn, in *Jupiter,* T. Gehrels, Ed. (Univ. of Arizona Press, Tucson, 1976), pp. 216–237; S. K. Atreya, T. M. Donahue, M. C. Festou, *Astrophys. J.* **747,** L43 (1981); stellar occultation results are reviewed by D. M. Hunten and J. Veverka, in *Jupiter,* T. Gehrels, Ed. (Univ. of Arizona Press, Tucson, 1976), pp. 247–283.
2. G. F. Lindal *et al., J. Geophys. Res.* **86,** 8721 (1981).
3. R. Hanel *et al., Science* **204,** 972 (1979); F. M. Flasar *et al., J. Geophys. Res.* **86,** 8759 (1981).
4. M. C. Festou *et al., J. Geophys. Res.* **86,** 5715 (1981).
5. W. M. Sinton, W. W. Macy, G. S. Orton, *Icarus* **42,** 86 (1980).
6. J. Caldwell *et al., Astrophys. J.* **234,** L155 (1979).
7. C. Bezanger, B. Bezard, D. Gautier, in *The Jovian Atmospheres,* NASA Conf. Publ. 244, M. A. Allison and L. D. Travis, Eds. (NASA, Washington, DC, 1986), pp. 79–81; Jupiter's (sidereal) orbital period is 11.86 years.
8. R. F. Beebe, R. M. Suggs, T. Little, *Icarus* **66,** 359 (1986).
9. B. J. Conrath, P. J. Gierasch, S. S. Leroy, *ibid.* **83,** 255 (1990).
10. R. D. Cess *et al., ibid.* **46,** 249 (1981).
11. J. Caldwell, A. T. Tokunaga, F. C. Gillett, *ibid.* **41,** 667 (1980); J. Caldwell, A. T. Tokunaga, G. S. Orton, *ibid.* **53,** 133 (1983); S. J. Kim *et al., ibid.* **64,** 233 (1985); R. Halthore *et al., ibid.* **74,** 331 (1988).
12. P. J. Gierasch, B. J. Conrath, J. A. Magalhaes, *ibid.* **67,** 444 (1986).
13. B. J. Conrath, P. J. Gierasch, N. Nath, *ibid.* **48,** 256 (1981).
14. D. G. Andrews, J. R. Holton, C. B. Leovy, *Middle Atmosphere Dynamics,* (Academic Press, Orlando, 1987).
15. S. K. Park and R. A. Schowengerdt, *Comput. Vision, Graphics, Image Process* **23,** 258 (1983).

16. We acknowledge the help of the JPL Supercomputing Project and the National Aerodynamic Simulator at the NASA Ames Research Center in performing extensive transmission calculations for the Jovian and telluric atmospheres, relevant to our 7.8-μm filter. We thank the staff and management of the Infrared Telescope Facility for their support, particularly site superintendent R. Koehler, and thank IRTF acting Division Chief E. Becklin and IRTF Division Chief R. Joseph for their effort to schedule a monthly monitoring program. We thank the IRTF telescope allocation committee for their long-term support for this research. We are grateful to programming help from I. M. Avruch, E. Russell, and M. Huie, who were all supported by California Institute of Technology Summer Undergraduate Research Fellowships at the Jet Propulsion Laboratory. We thank J. Klavetter for assistance with observing and data reduction during 1982. This research was sponsored by the National Aeronautics and Space Administration for work performed at the Jet Propulsion Laboratory, California Institute of Technology, and at the Institute for Astronomy, University of Hawaii; and by the National Research Council of Canada for work performed at York University. G.S.O., A.J.F., J.C., K.H.B., J.T.B., T.Z.M., and R.A.W. were visiting astronomers at the Infrared Telescope Facility which is operated by the University of Hawaii under contract to the National Aeronautics and Space Administration. G.S.O. particularly acknowledges support from the Galileo Project for this portion of his pre-encounter interdisciplinary investigation. These data were collected as one element of a larger set of observations coordinated by the International Jupiter Watch. They will be submitted to the Atmospheres Discipline Node of the Planetary Data System for archival and general reference.

20 December 1990; accepted 15 March 1991

A Class III Transcription Factor Composed of RNA

LISA S. YOUNG, HEATHER M. DUNSTAN, PAMELA R. WITTE, TIMOTHY P. SMITH, SIMONE OTTONELLO, KAREN U. SPRAGUE*

It is generally assumed that the machinery that transcribes genes is composed entirely of polypeptides. However, in vitro transcription by silkworm RNA polymerase III requires a transcription factor that is not a polypeptide. This component, TFIIIR, is distinct from the previously identified transcription components: RNA polymerase III, and the accessory factors TFIIIA, TFIIIB, TFIIIC, and TFIIID. The newly discovered TFIIIR is a macromolecule that appears to be composed of RNA. It is resistant to heat, detergent, phenol, protease, and deoxyribonuclease, but it is sensitive to alkali and ribonuclease.

THE PROMOTERS RECOGNIZED BY RNA POLYMERASE III require at least three transcription factors in addition to polymerase itself (*1–3*). These discrete and readily separable components appear to act as a unit during in vitro transcription of silkworm class III genes (*4–6*). Although protein-protein interactions could potentially account for the cooperative action of multiple transcription components, we considered the possibility that a nucleic acid might contribute to the structural integrity of the active RNA polymerase III transcription complex. While such a proposal has no precedent, a variety of other key biological processes such as protein synthesis, protein secretion, RNA processing, and telomere maintenance use machinery that is organized in ribonucleoprotein particles (*7–13*). We therefore set out to determine whether a nucleic acid, apart from the template, plays an essential role in transcription by silkworm RNA polymerase III.

We examined the sensitivity of the transcriptional activity of crude extracts to nuclease treatment in order to determine whether the RNA polymerase III transcription machinery includes an essential nucleic acid component. Micrococcal nuclease was chosen because its action can be stopped by EGTA-chelation of calcium ions—a procedure that does not interfere with subsequent assay of transcription activity in the treated extract. Micrococcal nuclease completely destroyed the ability of a silk gland nuclear extract to transcribe a gene coding for silkworm alanine transfer RNA ($tRNA_C^{Ala}$)(Fig. 1). Control experiments showed that loss of transcriptional activity requires the simultaneous presence of both calcium ions and micro-

L. S. Young, H. M. Dunstan, P. R. Witte, T. P. Smith, and K. U. Sprague are at the Institute of Molecular Biology, University of Oregon, Eugene, OR 97403. H. M. Dunstan and K. U. Sprague are affiliated with the Department of Biology and T. P. Smith with the Department of Chemistry. S. Ottonello is at the Instituto di Scienze Biochimiche, Universita di Parma, 43100 Parma, Italy.

*To whom correspondence should be addressed.